Optical phonons in isotope superlattices of GaAs, GaP, and GaSb studied by Raman scattering

A. Göbel, T. Ruf, A. Fischer, K. Eberl, and M. Cardona
Max-Planck-Institut für Festkörperforschung, Heisenbergstrasse 1, D-70569 Stuttgart, Germany

J. P. Silveira and F. Briones
Instituto de Microelectrónica de Madrid, Centro Nacional de Microelectrónica, CSIC, Calle Isaak Newton 8, E-28760 Tres Cantos Madrid, Spain

(Received 23 October 1998; revised manuscript received 2 February 1999)

We have investigated the LO-phonon Raman spectra of [100] oriented gallium isotope superlattices $(^{69}GaX)_n(^{71}GaX)_n$ [X=P,As; both elements have a single stable isotope] at low temperature. When the number of monolayers $2n$ within one superlattice (SL) unit cell is varied, anticrossings between phonons confined in the ^{69}GaX and ^{71}GaX layers are observed. We have used a planar bond-charge model to calculate the frequencies and intensities of the modes as a function of layer thickness. For the GaP isotope SL's, we find that a simulation of isotopically mixed interface layers is in good agreement with the experiment, while the assumption of ideal interfaces does not reproduce the data well. Spectra from the GaAs isotope SL's are substantially broadened compared to the LO phonon width in bulk samples, thus allowing only a qualitative discussion of phonon-confinement effects. Predictions for GaSb isotope SL's, in which both Ga *and* Sb isotopes can be substituted, are given. Raman spectra of bulk GaAs with varying gallium-isotope ratio are also discussed. [S0163-1829(99)04019-9]

I. INTRODUCTION

The vibrational properties of low-dimensional semiconductors, such as quantum wells and superlattices (SL's), have been studied intensively for many years.[1–4] Information about the lattice dynamics and the electron-phonon interaction is very important to understand the electronic and optical properties of devices based on such structures. The detailed knowledge about these phenomena has even been applied to make new devices, e.g., the quantum cascade laser.[5]

In most SL's, both the electronic structure *and* the phonons are strongly modified as compared to the bulk.[1–4] We have recently reported on a new kind of heterostructure: SL's made from different stable isotopes.[6–8] In this case, *only* the vibrational properties are affected by lowering the dimensionality while the electronic structure remains basically bulklike. Using Raman scattering, we have investigated phonons in SL's with the repeat sequence $^{70}Ge_n{}^{74}Ge_m$, where n and m give the number of atomic monolayers for the two isotopes. By varying the layer thicknesses we have observed interesting mode mixing and anticrossing effects, which are reflected in the Raman peak positions and the relative scattering intensities.[6] Such studies reveal details of the phonon displacement patterns. Furthermore, they provide sensitive tests of lattice-dynamical models and calculations of the Raman intensities. Information about interface properties, e.g., the mixing of isotopes and self-diffusion, can also be obtained.[6,9] In asymmetric isotope SL's, variations of modes associated with thin $^{70}Ge_2$ or $^{74}Ge_2$ layers have been investigated when the thickness of the respectively opposite material was varied.[4,10] This allows one to study a SL analog of light- or heavy-mass defects in semiconductors.

In the present paper we extend these investigations to isotope SL's made from *compound* semiconductors. For GaAs and GaP, only the gallium sublattice can be modulated (^{69}Ga, ^{71}Ga) since As and P are isotopically pure in the natural element. This leads to small isotope shifts of the bulk dispersions, and thus one expects that phonon confinement effects are more difficult to observe than in germanium isotope SL's. On the other hand, this approach yields valuable information on lattice-dynamical properties, e.g., the phonon displacement patterns, the validity of models for Raman intensities, and (isotope) mixing at the SL interfaces,[11] which justifies this effort. Theoretical predictions for GaSb isotope SL's, where both cations and anions can be isotopically substituted, are also presented. In these systems, SL's can be made by isotope mass variations of either the heavy- or the light-mass constituents. This is beyond the possibilities found in isotopic SL's made from elemental semiconductors.

Note that GaAs isotope SL's have been proposed in Ref. 12 and were already applied to study Ga self-diffusion in Ref. 13. Raman scattering is one of the few nondestructive techniques to investigate isotope SL's. Other methods, which have emerged recently, are resonant nuclear diffraction using synchrotron radiation[14] and neutron reflectometry.[15,16] While these techniques have so far been used mainly to investigate metallic SL's containing, e.g., different iron isotopes, their application to semiconductors is possible. It has been proposed[17] that multilayers containing ^{73}Ge could be used as ultranarrow-bandpass monochromators for synchrotron radiation at the low-energy nuclear resonance of this isotope at 13.3 keV. Germanium isotope SL's (Ref. 6) have been used in the first tests of the new neutron ''Advanced Diffractometer for the Analysis of Materials'' (ADAM) at the Institut Laue-Langevin, Grenoble, and their interface quality has been estimated.[15] Various possible applications of isotope SL's in optoelectronics and neutron optics have been discussed in Ref. 18.

The paper is organized as follows: In Sec. II we describe the experiment and the samples, while the simulations are

discussed in Sec. III. Section IV presents the experimental results and compares them to the predictions of the model calculation. The conclusions are drawn in Sec. V.

II. EXPERIMENT

A. Samples

We have investigated a series of isotope SL's in zinc-blende GaP and GaAs. Natural gallium has two stable isotopes, ^{69}Ga and ^{71}Ga, with 60.2% and 39.8% abundance, respectively, while phosphorus (^{31}P) and arsenic (^{75}As) are isotopically pure in nature. An isotope SL is formed when repeatedly stacking units of $(^{69}\mathrm{GaX})_n(^{71}\mathrm{GaX})_n$ upon each other, where X stands for either P or As, and n is the number of monolayers (ML). The growth direction for both materials is [100]. One monolayer is 2.75 Å (GaP) or 2.83 Å (GaAs) thick. The total SL thicknesses are between 4000 and 5000 Å for all samples. We have investigated GaP SL's with $n=4$, 6, 7, 8, 9, 10, 12, 13, 14, 16, 18, 20, 24, and 28 ML. The single-layer thicknesses of the GaAs SL's are $n=4$, 6, 8, 10, 12, and 14 ML. Besides the SL's, we have grown isotopically pure samples (^{69}GaP, ^{71}GaP, ^{69}GaAs, and ^{71}GaAs) as well as isotopically alloyed samples ($^{69}\mathrm{Ga}_{0.75}{}^{71}\mathrm{Ga}_{0.25}\mathrm{As}$, $^{\mathrm{nat}}$GaAs, $^{69}\mathrm{Ga}_{0.5}{}^{71}\mathrm{Ga}_{0.5}\mathrm{As}$, and $^{69}\mathrm{Ga}_{0.25}{}^{71}\mathrm{Ga}_{0.75}\mathrm{As}$) for reference purposes and to investigate isotope disorder effects, which will be published elsewhere.[19]

GaP SL's were grown in Madrid by standard molecular beam epitaxy (MBE), not by atomic-layer MBE or atomic-layer epitaxy, using conventional Knudsen cells for Ga and a valved cracker cell loaded with red phosphorous as a source for P_2. The individual layer thicknesses within the SL's were carefully controlled by means of reflection high-energy electron diffraction oscillations that were recorded during the whole growth procedure and used to activate the shutters in real time to assure an integer number of monolayers per period. This procedure was particularly necessary due to the poor thermal and, consequently, low growth rate stability of the Ga cells loaded with a very small amount, less then 1 gram, of isotopically pure elements. All samples were grown on undoped GaP(001) substrates at 700 °C. The growth rate was about 0.5 ML/s. To initiate good sample growth a 5000-Å thick buffer layer of natural GaP was deposited first in order to achieve an atomically flat smooth surface.

The GaAs SL's were fabricated in Stuttgart. They were grown by MBE, using low growth rates and standard Knudsen cells, at 580 °C on nominally intrinsic GaAs [100] substrates of natural isotopic composition. A 200–300-Å thick buffer layer of natural GaAs was grown first.

The source material for the epilayers has a nominal isotope purity of 99.6% for both gallium isotopes. While the P and As source materials were highly chemically pure, the chemical purity of the gallium source material was not as good as desired: In most GaAs samples the ^{71}Ga contained in total up to 2300-ppm impurities with Fe, Al, and Sn being the main ones, while the ^{69}Ga source material contained in total up to 1450 ppm of mainly Fe, Cr, and Sn. For three groups of specimens, namely the GaP samples, the $n=10$ and 12 GaAs SL's, and the ^{69}GaAs and ^{71}GaAs bulk samples, other gallium isotope batches were available as source material: The ^{71}Ga(^{69}Ga) source material for these samples contained a total of up to 1440 ppm (1230 ppm) impurities.

B. Raman measurements

All Raman spectra were recorded in back-scattering geometry with the sample temperature held at 8 K. We used the 413.1-nm krypton laser line to excite the spectra of the GaP samples and the 514.5 nm argon laser line for the GaAs samples. Excitation powers of up to 65 mW (GaP) and 100 mW (GaAs) in a point focus were used for most measurements. For the GaAs samples, we checked that a line focus together with a similar excitation power does not alter the spectra. Therefore, the effects of sample heating can be neglected for our purposes. The spectra were calibrated against nearby plasma lines of the respective laser, i.e., a line at 360.0 cm^{-1} (GaP) and one at 286.5 cm^{-1} (GaAs). An $f=0.85$ m double monochromator (model SPEX 1404) with 1800 groves/mm holographic gratings was used to disperse the scattered light. For the measurements of the GaP SL's we used a spectral resolution [full width at half maximum, (FWHM)] of 0.46 cm^{-1}. Resolutions of 0.63 and 1.24 cm^{-1} were used for the GaAs SL's. By measurements of very narrow plasma lines and of the laser line, we have checked that the instrumental resolution, at the slit widths used, is well approximated by a Gaussian line shape. Consequently, we have fitted all phonon spectra by Voigt profiles, in which the Gaussian widths were set to the above values. All values given are the average of two or three measurements on different spots of the samples.

III. PLANAR BOND-CHARGE MODEL

A. Lattice dynamics

The planar bond-charge model (PBCM) was used successfully before to fit the bulk phonon-dispersion curves of nonpolar (Si and Ge) as well as polar semiconductors (GaAs, AlSb, and GaSb).[20] It has also been applied to study phonons in Ge isotope SL's.[6,9] Because of its simplicity, we use this model in the following to calculate the lattice vibrations in isotope SL's made from *compound* semiconductors. When propagating along high-symmetry directions, i.e., [100] or [111], the longitudinal and transverse modes are decoupled. In Fig. 1, we schematically show this model with gallium cation and group-V element anion planes (X) as well as bond-charge planes (BCP) for phonon propagation along the [100] direction for a unit cell of a $(^{69}\mathrm{GaX})_2(^{71}\mathrm{GaX})_2$ SL. In the PBCM, planes perpendicular to the [100] axis move as rigid units and, as a result, the vibrational modes can be described by a linear-chain-like ansatz. Besides nearest- and next-nearest-neighbor force constants between the atomic (ionic) planes given by $k_{\pm 1}$ and $k_{\pm 2}^{\mathrm{Ga}}, k_{\pm 2}^{\mathrm{X}}$, respectively, the PBCM takes into account electronic degrees of freedom by introducing planes of nearly zero mass midway between the atomic planes.[20] These are the bond-charge planes (dashed lines). Their inclusion has proven useful to reproduce the flattening of the transverse acoustic modes at the Brillouin zone edge.[20,21] The force constants that couple the atomic planes to the BCP's are, in general, different for the coupling to anionic ($q_{\pm 1}^{\mathrm{X}}$) or cationic ($q_{\pm 1}^{\mathrm{Ga}}$) planes. For reasons of

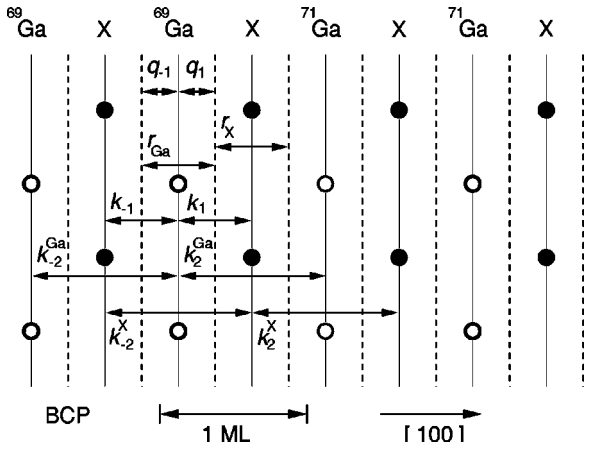

FIG. 1. Planar bond-charge model for isotope GaX SL's. A $(^{69}GaX)_2(^{71}GaX)_2$ SL unit cell along [100] is shown, and the size of one monolayer is indicated. The bond-charge planes (dashed lines) are located halfway between the ionic planes. The force constants used in the planar bond-charge model for propagation along the [100] direction are labeled.

simplicity, however, we take them to be identical in the following. In addition, the symmetry along the [100] axis requires q_1 to be equal to q_{-1} and $k_1 \equiv k_{-1}$. Furthermore, it is found[20] that the next-nearest-neighbor interaction, taken into account through the force constants $k^{\mathrm{Ga}}_{\pm 2}$ and $k^{\mathrm{X}}_{\pm 2}$, can be neglected for the propagation of longitudinal modes along the [100] axis, which is of interest here. In our model, 1 ML (one formula unit) consists of one gallium and one group-V element plane and two BCP's.

In order to simulate the Raman spectra of a particular isotope SL, we have generated its dynamical matrix taking a supercell approach.[20] The diagonalization of this matrix yields the vibrational frequencies and atomic displacements in the SL's. In Table I we give the force constants used in these calculations. Those for GaAs and GaSb are taken from Ref. 20. They were obtained from least-square fits to the longitudinal phonon dispersion determined by inelastic neutron scattering. The force constants for GaP were adjusted from those of GaAs such as to reproduce the Γ- and X-point frequencies at low temperature. Unfortunately, data from inelastic neutron scattering for the LO branch along the [100] axis are not available[22,23] for an independent determination of these force constants.

The new periodicity along the SL growth direction induces a backfolding of the Brillouin zone, so that additional phonon modes arise at the zone center. Since we have performed Raman backscattering measurements on the [100] surface of our samples, the modes stemming from the transverse-optic dispersions of the two bulk materials are not Raman active.[24] Those deriving from the longitudinal-optic (LO) dispersions of bulk ^{69}GaX and ^{71}GaX, however, can be Raman active. As an example, we discuss the case of GaP. In Fig. 2(a) we show the LO bulk dispersions of ^{69}GaP and ^{71}GaP. The arrow indicates the wave vector q for which the ^{69}GaP bulk dispersion drops below the Γ-point frequency of the ^{71}GaP LO bulk dispersion. Figure 2(b) shows the analogous GaAs bulk dispersions. According to the PBCM used here, the zone-center frequencies of the LO mode in the bulk materials are $\omega_\Gamma(^{69}\mathrm{GaP}) = 406.5\ \mathrm{cm}^{-1}$ and $\omega_\Gamma(^{71}\mathrm{GaP}) = 404.7\ \mathrm{cm}^{-1}$, so that there is a frequency gap of $1.8\ \mathrm{cm}^{-1}$ between the two bulk dispersions. Modes of the bulk ^{69}GaP LO dispersion, which lie inside this gap, are confined to the $(^{69}\mathrm{GaP})_n$ layer of the SL's, i.e., they show only little penetration of the phonon amplitude into the $(^{71}\mathrm{GaP})_n$ layers. In contrast, only the mode that corresponds to the ^{71}GaP bulk Raman mode can be regarded as confined in the SL's while the other modes of the ^{71}GaP bulk dispersion strongly mix with modes of the $(^{69}\mathrm{GaP})_n$ layer. The number of backfolded modes increases linearly with n, so that for large n one finds a large number of confined modes. The displacements of the confined modes alternately have even or odd parity with respect to a midlayer plane, and only the former are Raman active.[3] In the following, the modes in the layers are labeled according to the number of half wavelengths occurring within the layer having the respective Ga isotope, e.g., $^{69}LO_1$ (even parity), $^{69}LO_2$ (odd parity), $^{71}LO_1$ (even), $^{71}LO_2$ (odd), etc.

TABLE I. Force constants used in the planar bond-charge model for the propagation of longitudinal phonons along [100] in gallium-group-V semiconductors (units: N/m).

	GaP [a]	GaAs[20]	GaSb[20]
$q_{\pm 1}$	3044	3046	2910
r_{Ga}	36.0	38.6	38.5
r_{X}	47	54	26
$k_{\pm 1}$	−1418	−1432	−1381

[a]Adjusted from GaAs, see text.

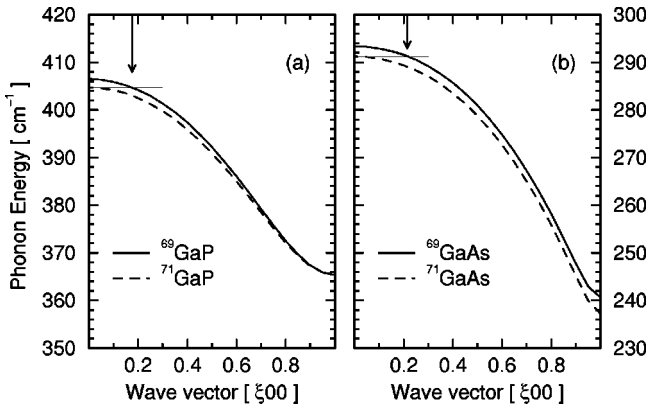

FIG. 2. Longitudinal optic phonon dispersion for bulk GaP (a) and bulk GaAs (b) containing pure ^{69}Ga and ^{71}Ga calculated with the PBCM. The arrows indicate the wave vector q at which the ^{69}GaX dispersion drops below the Γ-point value of the ^{71}GaX dispersion, i.e., the range of vanishing dispersion overlap $[q(^{69}\mathrm{GaP}) = 0.175$ r.l.u. and $q(^{69}\mathrm{GaAs}) = 0.215$ r.l.u.].

B. Raman intensities

The Raman intensities of phonons in isotope SL's can be calculated within the bond polarizability model assuming equal polarizabilities in both constituent materials.[1,6,25] They are proportional to the square of the sum of the relative atomic displacements, i.e.,

$$I \sim \left| \sum_{i=1}^{n} [u_i(^{69}\mathrm{Ga}) - u_i(\mathrm{X})] + \sum_{j=n+1}^{2n} [u_j(^{71}\mathrm{Ga}) - u_j(\mathrm{X})] \right|^2, \quad (1)$$

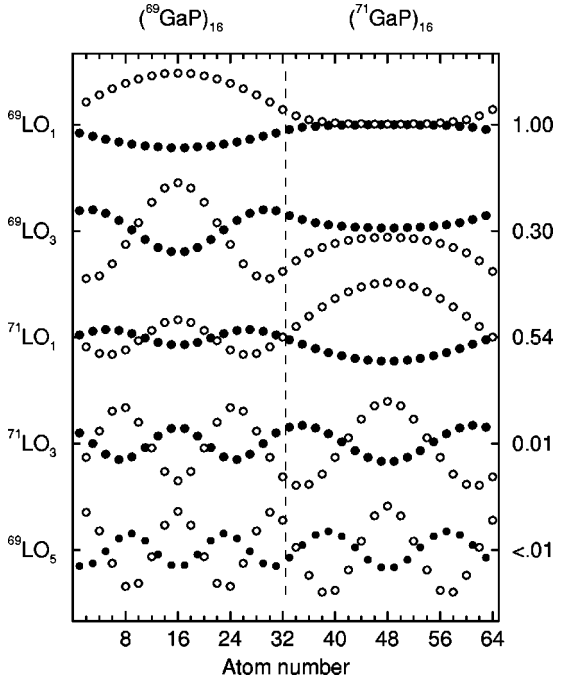

FIG. 3. The atomic displacements of odd-index LO modes in a $(^{69}GaX)_{16}(^{71}GaX)_{16}$ SL unit cell are shown. These Raman-active modes have even parity with respect to midlayer planes, which are at atom number 16 and 48 in this example. The Ga (filled dots) and P (open circles) atomic displacements are calculated using the PBCM for perfect interfaces (vertical dashed line). The labels on the left identify the predominant character of the mode, those on the right give the relative Raman intensities with respect to that of the $^{69}LO_1$ mode. The tick marks on the vertical axis indicate zero displacement of the respective mode.

where i,j label the ML's and u is the displacement of the atoms in the SL. The summation extends over the respective ML's of the two materials. As mentioned before, the even and odd parity modes alternate with decreasing frequency. However, when the size $2n$ of the SL unit cell decreases, $^{69}LO_x$ modes confined to the $(^{69}GaP)_n$ layers shift towards the energy of the $^{71}LO_1$ mode: As a result, modes with the same parity interact, the vibrations acquire a mixed character, and their labeling is not unambiguous. In some cases even more than two modes are strongly mixed.

In order to put the assignment on a well-defined footing, we have chosen the following procedure: In Fig. 3, we show the displacement patterns of the five Raman-active odd-index modes (even parity, see Sec. III A) with highest frequencies for a $(^{69}GaP)_{16}(^{71}GaP)_{16}$ SL with perfect interfaces. Examples for displacement patterns of even-index modes can be found, e.g., in Refs. 4 and 10. From the displacement amplitudes in the two layers, the mode assignment is rather straightforward for the $^{69}LO_1$, $^{69}LO_3$, and $^{71}LO_1$ modes if one considers that their index x corresponds, in a good approximation, to the number of half-wavelengths confined in the respective layers of either ^{69}GaP or ^{71}GaP, and takes some penetration of the phonon wave functions in the adjacent material into account. These assignments are further corroborated by the fact that the strongest displacement amplitudes, which determine the vibrational energies, are indeed found in ^{69}GaP for $^{69}LO_1$ and $^{69}LO_3$ and in ^{71}GaP for $^{71}LO_1$.

Unfortunately, the mode assignment is not so obvious for the $^{69}LO_5$ and $^{71}LO_3$ modes, which are strongly mixed with each other. This can be seen already in Fig. 3: both modes have strong displacements with approximately three half-wavelengths in the $^{71}GaP(\rightarrow{}^{71}LO_3)$ and five half-wavelengths in the $^{69}GaP(\rightarrow{}^{69}LO_5)$ layers. Calculating the individual contributions from the ^{69}GaP and ^{71}GaP layers, i.e., the two sums in Eq. (1) separately for $^{69}LO_5$ and $^{71}LO_3$ reveals that for both these modes the contribution from the $(^{71}GaP)_{16}$ layer to the Raman signal is larger than that from the $(^{69}GaP)_{16}$ layer. Therefore, the ratio of the contributions of the two individual layers to the Raman intensity is smaller than unity for both $^{69}LO_5$ and $^{71}LO_3$. We have thus assigned the $^{69}LO_5$ character to that mode for which this ratio is larger than for the other one. For all modes, in particular when they are strongly mixed, we have assigned their characters according to such a *relative* dominance in the contributions of either the ^{69}GaP or ^{71}GaP layers to the total Raman intensity. It is interesting to note that in Fig. 3 even for the $^{69}LO_3$ mode the major contribution to the total Raman intensity derives from the $(^{71}GaP)_{16}$ layer, an issue which will be addressed in Sec. IV B.

IV. RESULTS AND DISCUSSION

A. GaP isotope SL's

Raman spectra of the folded LO modes in our $(^{69}GaP)_n(^{71}GaP)_n$ isotope SL's and of the LO mode in bulk ^{69}GaP and ^{71}GaP are shown in Fig. 4. All spectra are normalized to the same height. We found LO frequencies of 407.09(06) and 405.28(06) cm^{-1} and widths of 0.40(05) and 0.43(05) cm^{-1} (FWHM) for the bulk ^{69}GaP and ^{71}GaP samples, respectively. To a very good approximation, the zone-center frequency of an optic phonon in a bulk zinc-blende structure varies like $\mu^{-1/2}$ upon isotope substitution, where the reduced mass μ is given by $\mu^{-1}=m_{\mathrm{Ga}}^{-1}+m_{\mathrm{P}}^{-1}$. The LO phonon frequencies we have determined for the nominally isotopically pure materials are in good agreement with this rule. The spectra have a symmetric Lorentzian line shape with a very low-intensity shoulder towards smaller (larger) phonon frequencies for $^{69}GaP(^{71}GaP)$, respectively. We attribute this shoulder to a small residual signal intensity stemming from the substrate, which has the natural isotopic composition. The narrow and symmetric line shapes give evidence of the good sample quality. In particular they show that the free-carrier density is low enough not to broaden or shift the LO phonon as a result of plasmon-phonon coupling.[26] Since the GaP samples were grown from the same source materials using the same process, we infer that this broadening mechanism is negligible for the SL's as well.

The spectra obtained from the SL's are shown in Figs. 4(a) and 4(b). The peaks are labeled A, B, and C to denote the $^{71}LO_1$, $^{69}LO_1$, and $^{69}LO_3$ mode, respectively. For a small number of ML's ($n=4$, 6, 7, and 8) the spectra are dominated by the $^{69}LO_1$ mode (B), and the $^{71}LO_1$ mode (A) exhibits only a small intensity. The latter mode acquires an appreciable intensity for $n\geqslant 9$. The vertical dotted lines in Fig. 4 represent the LO phonon frequencies in bulk ^{69}GaP and ^{71}GaP. The $^{69}LO_1$ mode in the $n=4$ SL is located approximately at the average frequency of the two bulk

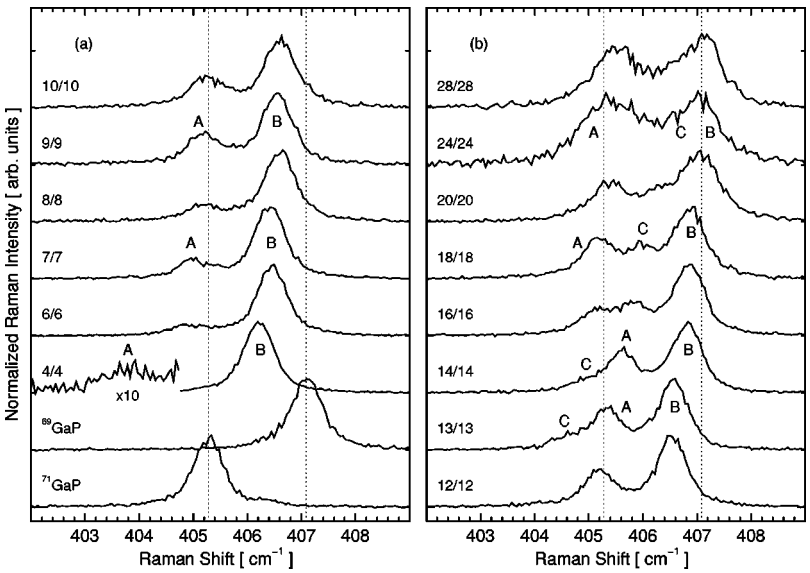

FIG. 4. Raman spectra of LO phonons in GaP isotope SL's and isotopically pure bulk samples obtained at 8 K. The vertical dotted lines indicate the frequencies of the bulk samples. The letters label the character of the modes: $^{71}LO_1$ (A), $^{69}LO_1$ (B), and $^{69}LO_3$ (C). See text for details.

samples. For larger SL unit cells it approaches the ^{69}GaP bulk value. The $^{71}LO_1$ (A) mode exhibits a similar trend, i.e., it approaches the frequency of the ^{71}GaP bulk mode, which it has essentially attained for $n=12$. However, for $n=13$ it can be seen that an additional mode C ($^{69}LO_3$) appears in the spectrum at a somewhat lower frequency. For $n=14$, the $^{69}LO_3$ mode (C) has increased in frequency and *pushed* the $^{71}LO_1$ mode to a value higher than the ^{71}GaP bulk frequency, a fact that indicates an anticrossing of the modes. If the modes merely crossed, this repulsion would not occur. For $n=16$ the two modes are strongly mixed, and for $n=18$ a three-peak structure emerges again, in which the $^{69}LO_3$ and $^{71}LO_1$ modes have exchanged their positions.

B. GaP: Comparison with theory

In order to discuss anticrossing effects as a function of layer thickness n, we now present the results of our simulation with the PBCM. Assigning the mode characters as defined in Sec. III, we show the mode frequencies and their relative Raman intensities as a function of n in Figs. 5(a) and 5(b), respectively. The $^{69}LO_x$ modes are shown as open symbols, while those having $^{71}LO_x$ character are displayed by the full symbols. The limiting bulk case of two semi-infinite ^{69}GaP and ^{71}GaP layers has only one Raman-active LO mode in each layer. Imposing periodic-boundary conditions on thinner layers leads to a backfolding of the bulk dispersion. This can be seen in Fig. 5(a) where, for the case of $n=42$, there are modes up to $^{69}LO_7$ folded into the dispersion gap. Decreasing the number of ML's leads to a larger SL mini-Brillouin zone and thus to a decrease in the $^{69}LO_x$ frequencies according to the bulk dispersion while the $^{71}LO_1$ frequency remains essentially constant. This causes mode anticrossings, e.g., near $n=34$, 24, and 12, in which the modes exchange their character and undergo a *jump* in frequency. From the simulation, we also find that once the $^{69}LO_x$ modes have anticrossed with the $^{71}LO_1$ mode, they undergo further anticrossings with the $^{71}LO_3$ and $^{71}LO_5$ modes, and their frequencies decrease rapidly with decreasing n. The frequency of the $^{69}LO_1$ mode decreases gradually for decreasing layer thicknesses and somewhat stronger for $n\leqslant 10$. This is in agreement with our experimental findings [compare peak B in Fig. 4(a)]. The decrease in the $^{71}LO_1$ mode frequency is very rapid for $n\leqslant 8$, which is a consequence of the increasing influence of backfolding effects for small layer thicknesses [compare peak A in Fig. 4(a)]. In the limit $n\rightarrow 1$ the $^{69}LO_1$ phonon remains the only Raman-active mode in the spectrum. Its frequency, located in between those for bulk ^{69}GaP and ^{71}GaP, and the mode displacements, however, indicate that it is no longer confined to ^{69}GaP but close to the *one* LO phonon expected in a bulk zinc-blende crystal with an average Ga mass. In this limit,

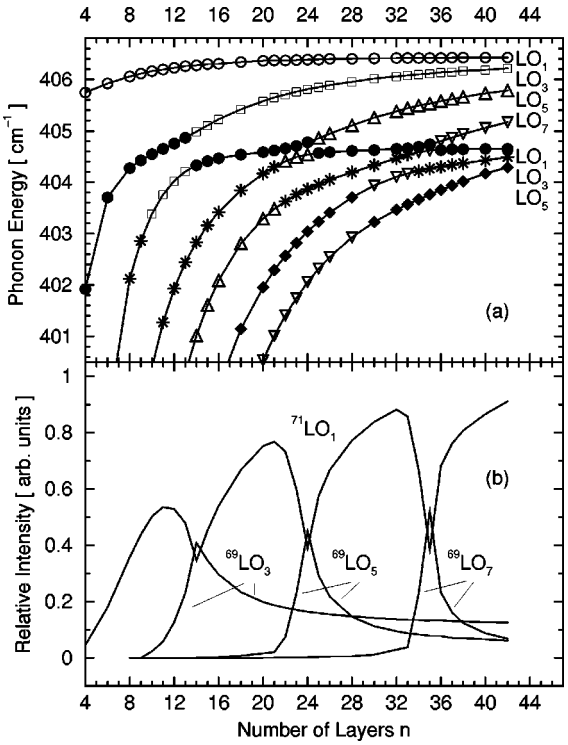

FIG. 5. (a) Energies and characters of odd-index LO phonon modes in GaP isotope SL's as calculated within the planar bond-charge model for the case of ideal interfaces. $^{69}LO_x$ modes are shown as open symbols; $^{71}LO_x$ modes as full symbols. (b) Calculated intensities of the modes relative to that of the $^{69}LO_1$ phonon.

$^{71}LO_1$ becomes equivalent to a backfolded zone-edge mode, which is not Raman active by symmetry; hence its vanishing intensity [see Figs. 4(a) and 5(b)].

Calculations for large supercell thicknesses $2n$ predict that the $^{69}LO_x$ intensities approach an intensity x^{-2} times that of the $^{69}LO_1$ mode. This reflects the increasing number of half-wavelengths (with adjacent ones scattering out of phase) in the displacement patterns with increasing x[4,6–10] and can be seen in Fig. 5(b) for $x=3$ or 5. For larger layer thicknesses the $^{69}LO_x$ frequencies become very similar to that of the $^{69}LO_1$ mode and, as a consequence of the anharmonic broadening, cannot be resolved from the latter mode in our experiment. However, with decreasing n, the $^{69}LO_7$, $^{69}LO_5$, and $^{69}LO_3$ modes acquire sizable intensities when they anticross with the $^{71}LO_1$ mode. They do not exhibit any intensity for even smaller layer thicknesses since beyond the anticrossing they are not confined anymore but propagate. This general trend can be seen in Fig. 4(b) where the $^{69}LO_3$ mode (peak C) anticrosses with the $^{71}LO_1$ mode (peak A).

From Fig. 5(b) it can also be seen that the $^{71}LO_1$ intensity increases towards that of the $^{69}LO_1$ mode for increasing n as one expects for the bulk limit where both modes should have similar intensities. Again, such a trend is actually observed in the spectra shown in Fig. 4(b). Qualitatively, this behavior arises from the fact that for large n both $^{69}LO_1$ and $^{71}LO_1$ modes are very much confined to their respective layers, and thus assume bulklike character. If, as for $^{71}LO_1$, mixing occurs, this mode couples to high-index $^{69}LO_x$ phonons which, due to the x^{-2} dependence of the Raman intensity, contribute only very weakly to the spectrum except in the close vicinity of the optimum-layer thickness for which an anticrossing occurs. For large n, the $^{71}LO_1$ phonon, therefore, does not lose or gain significant intensity by mode mixing.

We note that the spectrum of the $n=14$ SL [Fig. 4(b)] has a $^{71}LO_1$ mode (A) with an intensity that is considerably larger than that of the $^{69}LO_3$ mode (C). This is in contradiction with the results of the PBCM [compare Fig. 5(b)], where the two peaks are predicted to have the same intensity. This indicates that the model does not accurately reproduce the experimental findings when assuming perfectly sharp interfaces. An improved agreement is achieved when taking into account the effects of interface mixing: For this purpose, we assume that the gallium and phosphorous sublattices of the zinc-blende structure remain undistorted and elementally unmixed, so that *no structural or chemical disorder* occurs. For the Ga sublattice layers close to the interface, however, it seems reasonable that a mixing of the isotopes, i.e., *substitutional isotope disorder*, occurs. Assuming that the two cation layers on both sides of the anion interface are fully mixed, and thus have an average mass of a fictitious ^{70}Ga isotope, and that the adjacent cation layers are mixed in a one-to-three ratio, we obtain the masses 69, 69.5, 70, 70, 70.5, 71 for the six gallium layers at an $^{69}GaP/^{71}GaP$ interface. Using the PBCM for this mass distribution leads to predictions that are in better agreement with the experiment. They are discussed in the remainder of this subsection.

In Fig. 6 we show the Raman spectra for the $n=12$, 14, 16, and 18 SL's. A strong mixing of the $^{71}LO_1$ and $^{69}LO_3$ modes occurs for these layer thicknesses as a result of the mode anticrossing discussed above. We have fitted the spectra with three Voigt profiles using Gaussian widths fixed at the experimental resolution and Lorentzian widths taken the same for all peaks. The resulting fitted linewidths ($0.3-0.5$ cm^{-1}) are very close to the value of the anharmonic broadening determined from bulk samples. Thus, the peak positions, the common linewidth, and the intensity were used as fitting parameters. The dashed profiles indicate $^{69}LO_x$ modes while the full line displays the $^{71}LO_1$ mode and the resulting fit. The calculated mode frequencies are shown as vertical bars; they were shifted by a constant amount of $+0.4$ cm^{-1} for each spectrum, so that the $^{69}LO_1$ frequencies coincide. They were obtained using the PBCM, taking into account the isotope mixing at the interface as described above, and are in good agreement with the experiment. We note that the mode frequencies in the presence of mixed interfaces change only slightly (~ 0.2 cm^{-1}) when compared to those found for abrupt interfaces displayed in Fig. 5. Hence, we have shown that the spectra can be fitted rather well with a three-peak line shape for which the frequencies are in good agreement with both models, i.e., mixed or pure interfaces, and the linewidths are very similar to those observed in the bulk material. However, significant differences between the ideal and mixed interface scenarios occur when the Raman *intensities* are considered.

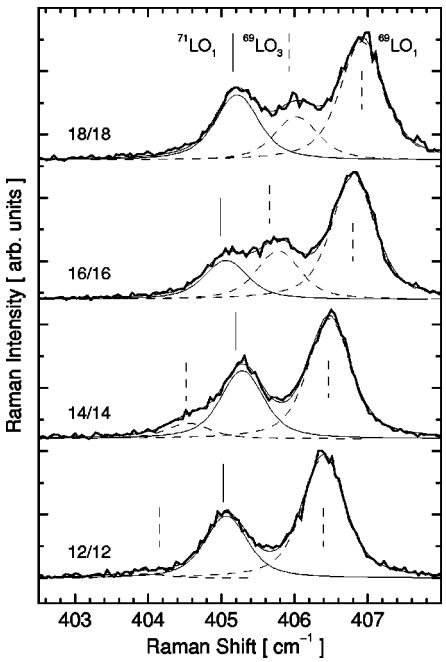

FIG. 6. Three-peak fits to the Raman spectra of GaP isotope SL's for $n=12$, 14, 16, and 18 obtained at 8 K. The positions, common widths, and intensities of the fitted Voigt profiles were used as adjustable parameters. The vertical lines display the frequencies calculated using the PBCM and taking interface mixing into account. The three individual fit components, as well as the total fit, are displayed by thin solid ($^{71}LO_1$), dashed ($^{69}LO_{1,3}$), and thin solid lines (total), respectively.

In Fig. 7 we show the calculated intensities of the $^{71}LO_1$, $^{69}LO_3$, and $^{69}LO_5$ modes for the case of ideal and mixed interfaces as solid and dashed lines, respectively. In the interface mixing scenario outlined above, the anticrossings of the $^{71}LO_1$ and $^{69}LO_x$ modes occur for larger n than they do for perfect SL's. This can be understood from a simple pic-

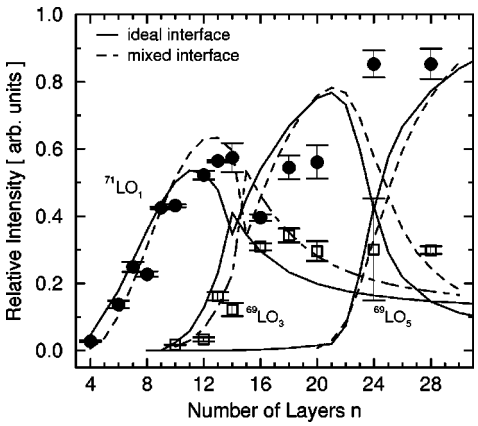

FIG. 7. Experimentally determined relative intensities of the confined phonons in GaP isotope SL's for the $^{71}LO_1$ (●) and $^{69}LO_3$ mode, (□) compared to that of the $^{69}LO_1$ mode which has been set to one. The solid lines show the calculations for ideal interfaces, while the dashed lines are predictions when the mixing of the two layers, on both sides of the P interface, is taken into account. See text for details.

ture: The admixture of light ^{69}Ga isotopes to the ideal ^{71}Ga layer results in an increase of the $^{71}LO_1$ mode frequency in Fig. 5(a). In the same way the $^{69}LO_x$ mode frequencies are lowered upon ^{71}Ga admixture to the ideal ^{69}Ga layers. As a result the anticrossings shift to larger n. The intensities obtained from fits to the experimental spectra are in good agreement with the proposed interface mixing for all SL's studied. They cannot be reconciled with the intensities of the abrupt interfaces. For SL thicknesses of $n \geqslant 18$ this agreement is no longer quantitative, most likely a consequence of using a three-peak fit for all spectra despite the fact that for $n \geqslant 18$ at least four modes acquire an appreciable intensity [compare Fig. 5(b)]. However, the lines are too close to each other to be resolved in the experimental spectra, so that in our fits the intensity stemming from the $^{69}LO_5$ mode is split up and inadvertently added to that of the $^{71}LO_1$ and $^{69}LO_3$ modes. The discrepancies in Fig. 7 for $n = 24$ and 28 between the calculated values for the interface mixing (dashed lines) and the fitted intensities (filled and open symbols) are accounted for in this way.

In summary, the PBCM together with the assumption of a mixing of Ga isotopes at the interfaces successfully describes the mode intensities, the anticrossings, and the frequencies of our GaP isotope SL-Raman spectra, as a function of layer-thickness n. Assuming ideal, i.e., abrupt interfaces, however, leads to discrepancies between the calculations and the observations.

C. GaAs isotope SL's

LO-phonon Raman spectra of isotopically pure and isotopically mixed bulk GaAs samples are shown in Fig. 8.[27] The phonon frequencies shift to lower values for larger isotope masses, and the line shapes are well described by symmetric Lorentzians. Here, we have used a short notation for the samples presented in Sec. II A, indicating the Ga isotope mixtures by their average mass.

In Fig. 9(a), we show the Raman shift of these samples as a function of the reduced mass. The LO frequencies of the

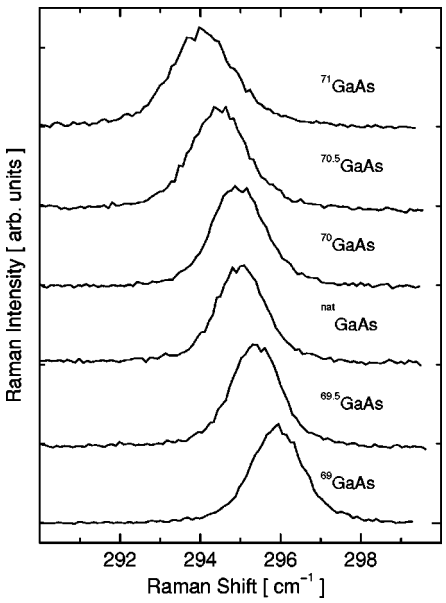

FIG. 8. Raman spectra of LO phonons in bulk GaAs samples of controlled isotopic composition obtained at 8 K.

^{69}GaAs, $^{69.5}$GaAs, ^{nat}GaAs, and ^{70}GaAs samples are in good agreement with the expected reduced-mass-like frequency shift ($\omega \sim \mu^{-1/2}$). In contrast, the frequencies of $^{70.5}$GaAs and ^{71}GaAs deviate from this behavior towards larger Raman shifts. There are, in principle, four reasons that could give rise to the deviations: (i) The actual isotopic composition of the $^{70.5}$GaAs and ^{71}GaAs samples could contain more ^{69}Ga than assumed. However, given the good isotopic purity of the source material used for the sample growth, this is unlikely. (ii) The LO phonons of the samples with a larger average gallium mass are more strongly renormalized by the

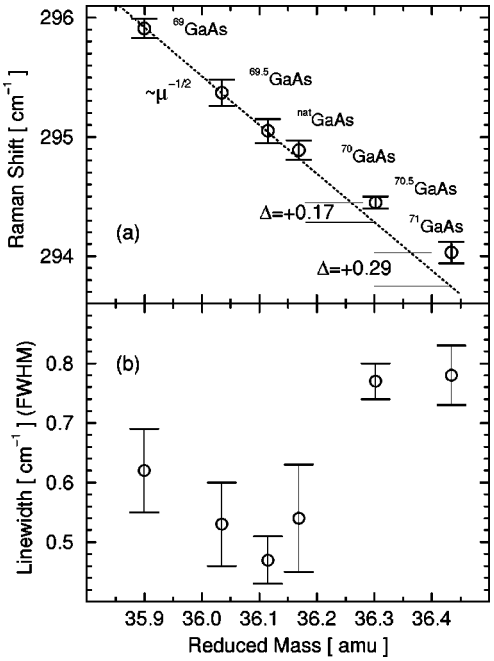

FIG. 9. Raman shift (a) and linewidth (b) of the LO phonon in bulk GaAs samples with controlled isotopic composition. The dashed line shows a reduced-mass-like behavior $\omega \sim \mu^{-1/2}$ fitted to the three lowest-μ samples only.

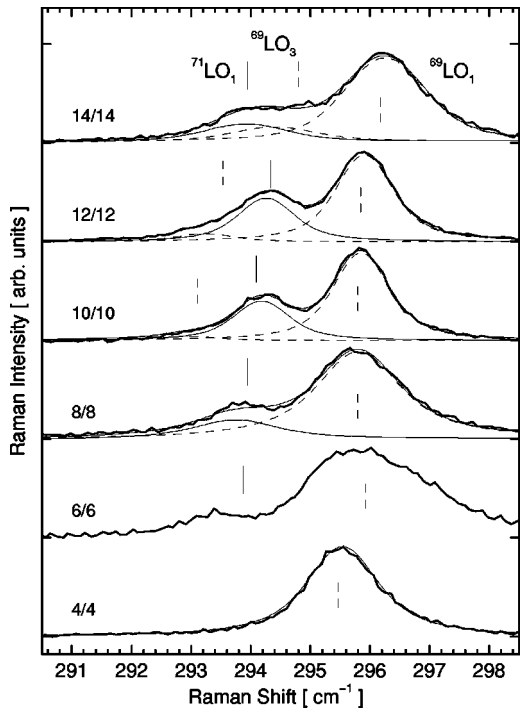

FIG. 10. Raman spectra of $(^{69}GaAs)_n(^{71}GaAs)_n$ SL's. Three ($n=14$, 12, 10), two ($n=8$), and one ($n=4$) peak fits to the spectra are shown. The fit to the $n=6$ spectrum is not shown since it is severely broadened, presumably due to plasmon-phonon coupling (see text). The vertical bars display the peak positions expected from the planar bond-charge model with interface mixing, shifted by $+3.0$ cm^{-1} such that the $^{69}LO_1$ mode frequencies coincide. The spectra were scaled to equal heights. The three individual fit components, as well as the total fit, are displayed by thin solid ($^{71}LO_1$), dashed ($^{69}LO_{1,3}$), and thin solid lines (total), respectively.

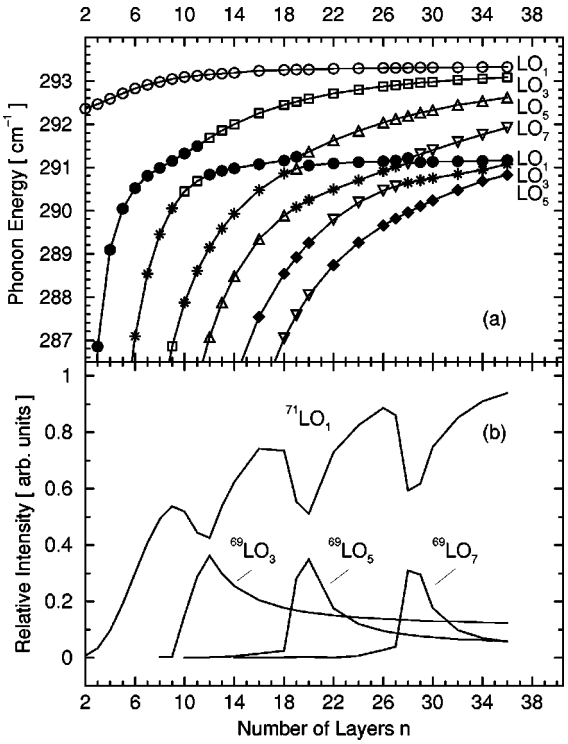

FIG. 11. (a) Energies and characters of phonon modes in GaAs isotope SL's as calculated within the planar bond-charge model for the case of ideal interfaces. (b) Intensities of the modes relative to that of the $^{69}LO_1$ phonon.

anharmonic interactions. This could arise if their frequencies fell into a range of a strong frequency dependence of the anharmonic interaction. We note, however, that this is unlikely since it should also lead to deviations[28] from the Lorentz form of the LO line shape, which are not observed. (iii) Isotope disorder-induced scattering can give rise to shifts of the phonon frequency.[29,30] However, the ^{71}GaAs is highly isotopically enriched, so that this effect has to be much smaller than in the case of ^{nat}GaAs, for which we do not observe an additional shift. (iv) The coupling of LO phonons to a longitudinal collective plasmon excitation, associated with free carriers in the material, leads to renormalized phonon frequencies.[26,31] For small carrier densities the LO phononlike mode is shifted towards larger energies. We find an increasing deviation from the reduced-mass behavior towards higher phonon energies with increasing ^{71}Ga concentration in the samples [compare Fig. 9(a)]. Furthermore, while the linewidths (FWHM) of the ^{69}GaAs, $^{69.5}$GaAs, ^{nat}GaAs, and ^{70}GaAs samples are on the average 0.54(10) cm^{-1}, those for $^{70.5}$GaAs and ^{71}GaAs are 0.78(10) cm^{-1}, as displayed in Fig. 9(b). Therefore, we are led to conclude, that the LO phonon frequencies of our GaAs samples with large ^{71}Ga content are affected by a small, albeit perceptible, plasmon-phonon coupling.

In Fig. 10, we show the Raman spectra obtained from the $(^{69}GaAs)_n(^{71}GaAs)_n$ SL's. The $^{69}LO_1$ mode for $n=4$ has a frequency of 295.5 cm^{-1}. It is somewhat lower than the ^{69}GaAs peak in Fig. 9(a). With increasing layer-thickness n its frequency increases towards the value found for bulk ^{69}GaAs. The peaks in the spectra obtained from the $n=4$, 6, and 8 SL's have linewidths of about $1.2-2.0$ cm^{-1} (FWHM). These widths are substantially larger than those found for the bulk samples (~ 0.6 cm^{-1}), which we conjecture to be due to plasmon-phonon coupling (see Sec. IV C). In contrast, the $n=10$, 12, and 14 SL's have smaller linewidths of about $0.6-0.8$ cm^{-1} (FWHM), an observation that suggests a better sample quality corresponding, presumably, to a lower free-carrier concentration.

D. GaAs: Comparison with theory

In Fig. 11(a) we show the LO frequencies in GaAs isotope SL's calculated using the PBCM under the assumption of ideal interfaces. The values obtained for the $^{69}LO_x$ modes are shown as open symbols, and those found for the $^{71}LO_x$ modes are displayed by filled symbols. The results are similar to those presented above for GaP isotope SL's. For $n=36$, the $^{69}LO_{1-7}$ modes are confined to the ^{69}GaAs layer. Reducing the number of ML's decreases their frequencies. They successively anticross with the $^{71}LO_1$ mode and further continue to anticross with the $^{71}LO_3$ and $^{71}LO_5$ modes. At thicknesses for which they strongly couple to the $^{71}LO_1$ phonon, they acquire a sizable intensity from the latter mode, and for even smaller n their oscillator strength vanishes. This is shown in Fig. 11(b).

A more detailed calculation of the mode intensities is shown in Fig. 12 for three cases: (i) perfect interfaces (solid lines); (ii) complete mixing of one gallium layer at the inter-

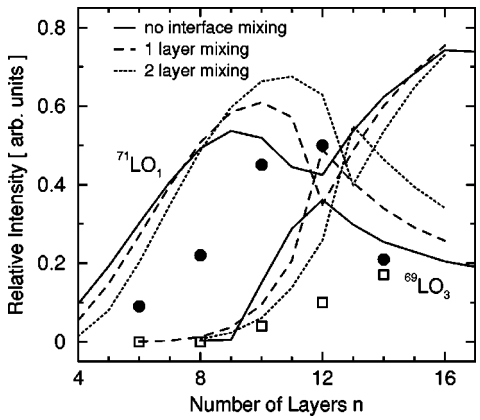

FIG. 12. Experimentally determined intensities of confined phonons in GaAs isotope SL's including the $^{71}LO_1$ (●) and $^{69}LO_3$ mode (□) relative to the $^{69}LO_1$ mode whose intensity is set to one. The solid line shows the calculated values for the case of ideal interfaces, while the dashed and dotted lines display results for two degrees of interface layer mixing. See text for details.

face (gallium mass sequence: 69, 70, 70, 71; dashed lines); and (iii) two-layer mixing at the interface (gallium mass sequence: 69, 69.5, 70, 70, 70.5, 71; dotted lines). It can be seen that the isotope mixing at the interfaces shifts the anticrossing of the $^{69}LO_3$ and $^{71}LO_1$ modes to larger SL thicknesses as discussed above for GaP. In addition, we show in Fig. 12 the relative intensities of the $^{71}LO_1$ (filled dots) and $^{69}LO_3$ (open squares) modes, which we have obtained from our fits to the experiment (compare Fig. 10). The measured relative intensities qualitatively agree with the predictions: That of $^{71}LO_1$ strongly increases with increasing n while the $^{69}LO_3$ signal becomes stronger only for larger periods. The equal relative intensities for $n=14$ suggest an anticrossing of these modes around this layer thickness. However, the data cannot be described quantitatively even when different interface mixing profiles are considered. This is attributed to sample imperfections whose origin remains to be clarified. Note that a comparison of theoretical spectra calculated for perfect interfaces with the Raman data is shown in Fig. 2.31 of Ref. 4.

E. GaSb

While P and As have only one isotope that occurs naturally, Sb has two natural isotopes (abundances: ^{121}Sb: 57.36%, ^{123}Sb: 42.64%). The trend towards heavier anions in the series GaP, GaAs, and GaSb results in a change of confinement conditions: While in GaP the SL periodicity is imposed by the *heavier* element, Ga as the *lighter* ion causes the SL periodicity in GaAs isotope SL's. In GaSb, an isotope SL can be achieved in two different ways: Substituting Ga now means that the lighter atom defines the SL, as in GaAs SL's, while the use of Sb isotopes means that the SL is defined by the heavier atom, analogous to the case of Ga replacement in GaP. The bulk LO zone-center frequencies of $^{69}Ga^{nat}Sb$ and $^{71}Ga^{nat}Sb$ differ by 2.4 cm^{-1}. As a result, the mode energies, in particular of $^{69}LO_3$ and $^{71}LO_1$, at layer thicknesses for which the anticrossing occurs, are spread out somewhat further than in GaP and GaAs. Therefore, the folded modes should be well resolved in high-quality

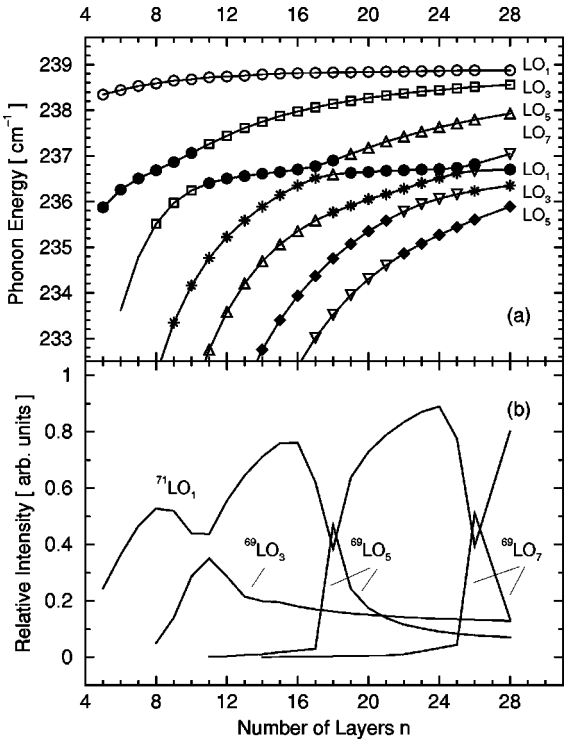

FIG. 13. (a) Energies and characters of phonon modes in $(^{69}Ga^{nat}Sb)_n(^{71}Ga^{nat}Sb)_n$ isotope Sl's as calculated within the planar bond-charge model for the case of ideal interfaces. (b) Intensities of the modes relative to that of the $^{69}LO_1$ phonon.

samples. Predictions of mode energies, characters, and intensities in GaSb isotope SL's $(^{69}Ga^{nat}Sb)_n(^{71}Ga^{nat}Sb)_n$ are shown in Fig. 13. Note that the range of vanishing dispersion overlap can be further enhanced by using appropriate Sb isotopes, e.g., to 2.9 cm^{-1} for $(^{69}Ga^{121}Sb)_n(^{71}Ga^{123}Sb)_n$ SL's.

V. SUMMARY AND CONCLUSION

Isotope substitution is an excellent means to change the energies of vibrational excitations of a crystal. Since the lattice-dynamical force constants remain unchanged upon isotope substitution, it also provides an excellent way to create SL's with uniform, i.e., bulklike electronic properties but a strong modulation of the vibronic properties.

We have presented Raman spectra of symmetric isotope SL's made from GaP and GaAs. The folded mode frequencies and their intensities are compared to simulations employing a planar bond-charge model. These calculations yield intensities that are in disagreement with the observations under the assumption of perfect interface layers. However, experiment and theory can be reconciled when interface isotope mixing of up to two layers is taken into account. Therefore, the Raman measurements are a sensitive and useful method to investigate the degree of interface layer mixing in the direction parallel to the growth axis.

Raman experiments on tempered SL's, in analogy to those published recently for Ge,[9] should be performed to complement recent self-diffusion investigations by secondary-ion mass spectroscopy on isotope heterostructures with much larger layer thicknesses.[13,33] Eventually, this might lead to a better characterization of the initial isotope

mixing at the SL interfaces, which occurs already during sample growth.

Another candidate where both anion and cation isotope replacement is possible is GaN. Raman experiments on bulk samples made from ^{14}N and ^{15}N have been reported recently;[34] they could be extended to GaN isotope SL's. This would be of interest since such structures should also exhibit a modulation of the electronic structure due to the much larger gap shifts expected for nitrogen substitution than, e.g., gallium replacement in GaAs.[32]

ACKNOWLEDGMENTS

We are indebted to F. Widulle for a critical reading of the manuscript, and to O. Buresch, who analyzed the chemical purity of the gallium-isotope source material.

[1] A. S. Barker, Jr., J. L. Merz, and A. C. Gossard, Phys. Rev. B **17**, 3181 (1978).
[2] C. Colvard, T. A. Gant, M. V. Klein, R. Merlin, R. Fischer, H. Morkoç, and A. C. Gossard, Phys. Rev. B **31**, 2080 (1985).
[3] B. Jusserand and M. Cardona, in *Light Scattering in Solids V*, edited by M. Cardona and G. Güntherodt, Topics in Applied Physics Vol. 66 (Springer, Heidelberg, 1989), p. 49.
[4] T. Ruf, *Phonon Raman Scattering in Semiconductors, Quantum Wells and Superlattices—Basic Results and Applications*, Springer Tracts in Modern Physics Vol. 142 (Springer, Heidelberg, 1998).
[5] J. Faist, F. Capasso, D. L. Sivco, C. Sirtori, A. L. Hutchinson, and A. Y. Cho, Science **264**, 553 (1994).
[6] J. Spitzer, T. Ruf, M. Cardona, W. Dondl, R. Schorer, G. Abstreiter, and E. E. Haller, Phys. Rev. Lett. **72**, 1565 (1994).
[7] M. Cardona, in *Festkörperprobleme/Advances in Solid State Physics*, edited by R. Helbig (Vieweg, Braunschweig/Wiesbaden, 1994), Vol. 34, p. 35.
[8] T. Ruf, H. D. Fuchs, and M. Cardona, Phys. Bl. **52**, 1115 (1996).
[9] E. Silveira, W. Dondl, G. Abstreiter, and E. E. Haller, Phys. Rev. B **56**, 2062 (1997).
[10] J. Spitzer, Ph.D. dissertation, Universität Stuttgart, 1994.
[11] E. Molinari, S. Baroni, P. Giannozzi, and S. de Gironcoli, Phys. Rev. B **45**, 4280 (1992).
[12] A. Ishibashi, in *Spectroscopy of Semiconductor Microstructures*, Vol. 206 of *NATO Advanced Study Institute, Series B: Physics*, edited by G. Fasol, A. Fasolino, and P. Luigli (Plenum, New York, 1989), p. 21.
[13] L. Wang, L. Hsu, E. E. Haller, J. W. Erickson, A. Fischer, K. Eberl, and M. Cardona, Phys. Rev. Lett. **76**, 2342 (1996).
[14] A. I. Chumakov, G. V. Smirnov, A. Q. R. Baron, J. Arthur, D. E. Brown, S. L. Ruby, G. S. Brown, and N. N. Salashchenko, Phys. Rev. Lett. **71**, 2489 (1993).
[15] A. Magerl and T. Ruf (unpublished).
[16] A. Schreyer, R. Siebrecht, U. Englisch, U. Pietsch, and H. Zabel, Physica B **248**, 349 (1998).
[17] V. Shvyd'ko and A. I. Chumakov (private communication).
[18] A. A. Berezin, Solid State Commun. **65**, 819 (1988).
[19] For a preliminary account of these studies see F. Widulle, T. Ruf, A. Göbel, I. Silier, E. Schönherr, M. Cardona, J. Camacho, A. Cantarero, W. Kriegseis, and V. I. Ozhogin, Physica B **263/264**, 353 (1999).
[20] P. Molinàs-Mata, A. J. Shields, and M. Cardona, Phys. Rev. B **47**, 1866 (1993); P. Molinàs-Mata and M. Cardona, *ibid.* **43**, 9799 (1991).
[21] W. Weber, Phys. Rev. B **15**, 4789 (1977).
[22] J. L. Yarnell, J. L. Warren, and R. G. Wenzel, in *Neutron Inelastic Scattering*, Symp. Copenhagen 1968 (IAEA, Vienna, 1969), Vol. I, p. 301.
[23] H. Bilz and W. Kress, in *Phonon Dispersion Relations in Insulators*, edited by M. Cardona and P. Fulde, Springer Series in Solid-State Sciences Vol. 10 (Springer, Heidelberg, 1979).
[24] *Light Scattering in Solids V* (Ref. 3), pp. 69–72.
[25] *Light Scattering in Solids V* (Ref. 3), p. 91.
[26] G. Abstreiter, M. Cardona, and A. Pinczuk, in *Light Scattering in Solids IV*, edited by M. Cardona and G. Güntherodt, Topics in Applied Physics Vol. 54 (Springer, Heidelberg, 1984), p. 5.
[27] These samples were also used for the investigation of the dependence of the fundamental electronic gap of GaAs on the isotope mass in Ref. 32.
[28] B. A. Weinstein, Solid State Commun. **20**, 999 (1979).
[29] S.-I. Tamura, Phys. Rev. B **30**, 849 (1984).
[30] A. Göbel, T. Ruf, J. M. Zhang, R. Lauck, and M. Cardona, Phys. Rev. B **59**, 2749 (1999).
[31] H. R. Chandrasekhar and A. K. Ramdas, Phys. Rev. B **21**, 1511 (1980).
[32] N. Garro, A. Cantarero, M. Cardona, A. Göbel, T. Ruf, and K. Eberl, Phys. Rev. B **54**, 4732 (1996).
[33] L. Wang, J. A. Wolk, L. Hsu, E. E. Haller, J. W. Erickson, M. Cardona, T. Ruf, J. P. Silveira, and F. Briones, Appl. Phys. Lett. **70**, 1831 (1997).
[34] J. M. Zhang, T. Ruf, M. Cardona, O. Ambacher, M. Stutzmann, J.-M. Wagner, and F. Bechstedt, Phys. Rev. B **56**, 14 399 (1997).